Stem Cell Research (2013) 11, 806–819

Available online at www.sciencedirect.com

SciVerse ScienceDirect

www.elsevier.com/locate/scr

Cardiolipin deficiency affects respiratory chain function and organization in an induced pluripotent stem cell model of Barth syndrome☆

Jan Dudek[a,1], I-Fen Cheng[b,c,1], Martina Balleininger[a], Frédéric M. Vaz[d], Katrin Streckfuss-Bömeke[b,c], Daniela Hübscher[b,c], Milena Vukotic[a], Ronald J.A. Wanders[d], Peter Rehling[a,e,*], Kaomei Guan[b,c,**]

[a] Department of Biochemistry II, University Medical Center Göttingen, Humboldtallee 23, 37073 Göttingen, Germany
[b] Department of Cardiology and Pneumology, University Medical Center Göttingen, Robert-Koch-Str. 40, 37075 Göttingen, Germany
[c] DZHK (German Center for Cardiovascular Research), partner site Göttingen, Germany
[d] Laboratory Genetic Metabolic Diseases, Academic Medical Center, University of Amsterdam, Amsterdam, The Netherlands
[e] Max-Planck Institute for Biophysical Chemistry, Am Faßberg 11, 37077 Göttingen, Germany

Received 11 January 2013; received in revised form 3 April 2013; accepted 15 May 2013
Available online 28 May 2013

Abstract Barth syndrome (BTHS) patients carrying mutations in *tafazzin* (*TAZ1*), which is involved in the final maturation of cardiolipin, present with dilated cardiomyopathy, skeletal myopathy, growth retardation and neutropenia. To study how mitochondrial function is impaired in BTHS patients, we generated induced pluripotent stem cells (iPSCs) to develop a novel and relevant human model system for BTHS. BTHS–iPSCs generated from dermal fibroblasts of three patients with different mutations in *TAZ1* expressed pluripotency markers, and were able to differentiate into cells derived from all three germ layers both in vitro and in vivo. We used these cells to study the impact of tafazzin deficiency on mitochondrial oxidative phosphorylation. We found an impaired remodeling of cardiolipin, a dramatic decrease in basal oxygen consumption rate and in the maximal respiratory capacity in BTHS–iPSCs. Simultaneous measurement of extra-cellular acidification rate allowed us a thorough assessment of the metabolic deficiency in BTHS patients. Blue native gel analyses revealed that decreased respiration coincided with dramatic structural changes in respiratory chain supercomplexes leading to a massive increase in generation of reactive oxygen species. Our data demonstrate that BTHS–iPSCs are capable of modeling BTHS by recapitulating the disease phenotype and thus are important tools for studying the disease mechanism.

* Correspondence to: P. Rehling, Department of Biochemistry II, University Medical Center Göttingen, Humboldtallee 23, 37073 Göttingen, Germany. Fax: +49 551 395979.
** Correspondence to: K. Guan, Department of Cardiology and Pneumology, University Medical Center Göttingen, Robert-Koch-Str. 40, 37075 Göttingen, Germany. Fax: +49 551 398124.
E-mail addresses: Peter.Rehling@medizin.uni-goettingen.de (P. Rehling), kguan@med.uni-goettingen.de (K. Guan).
[1] These authors contributed equally.

1873-5061/$ - see front matter © 2013 The Authors. Published by Elsevier B.V. All rights reserved.
http://dx.doi.org/10.1016/j.scr.2013.05.005

Introduction

Barth syndrome (BTHS, MIM# 302060) is a recessive disorder characterized by dilated cardiomyopathy, attended with skeletal myopathy, neutropenia, growth retardation and increased urinary excretion of 3-methylglutaconic acid in early childhood (Barth et al., 1983; Spencer et al., 2005; Takeda et al., 2011). The disease-causing gene was mapped to the *TAZ1* locus in the q28 region of the X chromosome (Xq28) encoding for the mitochondrial protein tafazzin. Tafazzin is an evolutionary conserved CoA independent phospholipid acyltransferase, involved in remodeling of cardiolipin (CL), the hallmark lipid of mitochondria (Neuwald, 1997; Xu et al., 2006). CL is a constituent of the inner (75%) and outer (25%) membranes where it plays pleiotropic roles in the maintenance of membrane complexes and cristae morphology (Xu et al., 2005; Acehan et al., 2007; Gebert et al., 2009). After its synthesis CL is deacylated to monolysocardiolipin (MLCL) and subsequently reacylated by tafazzin. This remodeling process maintains the normal content and composition of cardiolipin in mitochondria. Although tafazzin is ubiquitously expressed in all human tissues, the remodeled molecular species of cardiolipin are cell-type and tissue specific. Heart and skeletal muscle, tissues that require high mitochondrial metabolic activity, contain mainly tetra-linoleoyl-CL ($(C18:2)_4$-CL) in mitochondria whereas a broader species composition is found in other tissues, especially in the brain (Schlame et al., 2003; Schlame et al., 2002; Valianpour et al., 2002; Mckenzie et al., 2006; Houtkooper et al., 2009). It has been suggested that the different molecular species of cardiolipin observed in different cells and tissues are tailored to match the functional requirements and/or energetic demands of that cell or tissue (Houtkooper et al., 2009).

Respiratory chain complexes are organized into higher oligomeric structures called supercomplexes or respirasomes. In mammalian cells, complex I (NADH:ubiquinone oxidoreductase) is associated with dimeric complex III (ubiquinol: cytochrome *c* oxidoreductase) and multiple copies of complex IV (cytochrome *c* oxidoreductase) (Schägger and Pfeiffer, 2001; Schägger and Pfeiffer, 2000; Moreno-Lastres et al., 2012). The formation of supercomplexes was suggested to increase efficiency of respiration and prevent the generation of reactive oxygen species (Acín-Pérez et al., 2008; Vukotic et al., 2012; Strogolova et al., 2012; Chen et al., 2012). CL binding has been shown for all individual complexes of the respiratory chain and available crystal structures reveal CL in critical positions in complexes III and IV and the ADP–ATP carrier (Schwall et al., 2012; Shinzawa-Itoh et al., 2007; Lange et al., 2001; Pebay-Peyroula et al., 2003). CL molecules at the interface between individual complexes are thought to be essential for assembly of these complexes into supercomplexes (Brandner et al., 2005; Zhang et al., 2002; Wenz et al., 2009; Pfeiffer et al., 2003; Zhang et al., 2005; Bazán et al., 2012). Previous studies show that cardiomyocytes contain a unique composition of CL-dependent membrane complexes. A well-studied example is the respiratory chain complex IV with its cardiac tissue-specific subunits VIa, VIIa and VIII (Bachman et al., 1997; Grossman and Lomax, 1997; Arnaudo et al., 1992; Lomax et al., 1995). Experiments with yeast as a model organism or lymphoblasts from BTHS patients showed destabilization of respiratory chain supercomplexes in these cells and a decrease in respiratory chain activity in fibroblasts from BTHS patients (Mckenzie et al., 2006; Barth et al., 1996; Sedlák and Robinson, 1999).

Although mitochondrial respiratory dysfunction and destabilization of supercomplexes have been reported in fibroblasts or lymphoblasts from BTHS patients, it has remained open how these individual effects integrate into cellular metabolism, and how the different mutations in the tafazzin gene influence the cardiolipin composition and mitochondrial function in different cells and tissues.

To address the pathological changes of cardiac function in a suitable model system, a tafazzin knock down mouse model has been designed. However, the late onset of the cardiac phenotype after 8 months in adult mice did not reflect the early onset of the disease in human and raised the question of how well a mouse model resembles the situation in human tissue (Acehan et al., 2011; Soustek et al., 2011; Phoon et al., 2012). The recent successes in generation of human induced pluripotent stem cells (iPSCs) allow us modeling a disease in a culture dish, which is based on the unique capacity of these cells to continuously self-renew and to give rise to all cell types in the human body (Robinton and Daley, 2012). Indeed, there have been a number of studies reporting on the successful in vitro modeling of diseases using iPSCs generated from patients with a full range of genetically inherited as well as sporadic diseases (Wu and Hochedlinger, 2011).

In this study we therefore aimed to establish a human iPSC model system from dermal fibroblasts of BTHS patients. We found an impaired CL remodeling in BTHS–iPSCs, which recapitulates the disease phenotype. Assessment of mitochondrial function revealed a dramatic decrease in mitochondrial oxygen consumption in BTHS–iPSCs compared to control cells, which was not compensated by increased glycolysis. We found that structural changes in the respiratory chain supercomplexes are causing defects in energetic coupling and an increase of reactive oxygen species (ROS), thus, providing a possible explanation for the pathogenesis of the disease.

Material and methods

Generation and culture of BTHS–iPSCs

The study was approved by the ethical commission of Universitätsmedizin Göttingen. Dermal fibroblasts were obtained from 3 patients diagnosed with BTHS (Table 1) and 1 healthy donor (Houtkooper et al., 2009). Cells were grown in Dulbecco's Modified Eagle's Medium (DMEM; Invitrogen) containing 10% inactivated fetal bovine serum (FBS, Sigma), 2 mM L-glutamine (Invitrogen), 1× Non-Essential Amino Acid (NEAA; Invitrogen), and 50 μM β-mercaptoethanol (Serva). For transduction of dermal fibroblasts into iPSCs, a standardized protocol was applied as previously described (Streckfuss-Bomeke et al., 2012). Briefly, fibroblasts were infected with the lentivirus encoding all four human transcription factors OCT4, SOX2, KLF4 and c-MYC using the STEMCCA system and cultivated on mitomycin C-inactivated mouse embryonic fibroblasts (MEFs) in human iPSC medium composed of DMEM/F12 (Invitrogen) containing 20% knockout serum replacement (Invitrogen), 1× NEAA, 50 μM β-mercaptoethanol and 10 ng/ml basic fibroblast growth factor (bFGF, Peprotech)

Table 1 Information of patients, and patient-specific iPSC lines.

BTHS patient	DNA mutation	Protein	Type of mutation	ID of iPSC lines	Phenotype [a]	Primers used for mutation detection	Reference
TAZ10	590 G>T	Gly197Val	Missense	TAZ10-3 TAZ10-4	Severe	f: 5′GAA TTG AAC TGG AGG ATG TC-3′ r: 5′TCC CTG TCT ATG TTC CAC TC-3′	Houtkooper et al. (2009)
TAZ13	110-1 AG>AC	r.spl. Ex2del?	Splice site	TAZ13-2 TAZ13-3 TAZ13-4	Severe	f: 5′TGC TTC TGG ACC AGT GAG T-3′ r: 5′AGC CAC AAA TCC AAG TCT C-3′	Houtkooper et al. (2009)
TAZ15	170 G>T	Arg57Leu	Missense	TAZ15-1 TAZ15-5 TAZ15-8	Mild	f: 5′TGC TTC TGG ACC AGT GAG T-3′ r: 5′AGC CAC AAA TCC AAG TCT C-3′	Newly recruited

[a] All patients were diagnosed with BTHS on the basis of (ML)CL analysis of fibroblasts.

until iPSC colonies could be manually picked. The generated iPSCs were passaged using collagenase IV (200 U/ml, Worthington), gently scraped off with a cell scraper and then propagated on MEFs in human iPSC medium with medium change every day at 37 °C with 5% CO_2. Human embryonic stem cells (ESCs) HES3 served as a control (Streckfuss-Bomeke et al., 2012).

Genomic sequencing

The presence of the *TAZ1* mutations in the BTHS–iPSCs and their absence in the control iPSCs was verified by polymerase chain reaction-based sequencing of genomic DNA isolated from iPSCs using Maxwell® 16 DNA purification kit (Promega). The primer sets used for sequencing were given in Table 1.

Pluripotency characterization of iPSCs

The generated iPSCs were characterized for their pluripotency by alkaline phosphatase staining, and expression of pluripotency markers OCT4, SOX2, NANOG, LIN28, SSEA-4, and TRA-1-60 using RT-PCR analysis and immunofluorescence staining. Primer sequences and antibodies used have been described previously (Streckfuss-Bomeke et al., 2012). The DNA methylation analysis of the promoter regions of OCT4 and NANOG was conducted using bisulfite sequencing assays by Epigenomics (Berlin) as described in Streckfuss-Bomeke et al. (2012). Spontaneous iPSC differentiation in vitro was carried out via embryoid body formation as described in (Streckfuss-Bomeke et al., 2012). The developmental potential of generated iPSCs in vivo was studied by teratoma formation after subcutaneous injection of iPSCs (about 2 × 6-cm dishes at 70% confluence for each mouse) into 8-week-old $RAG2^{-/-}\gamma c^{-/-}$ immunodeficient mice. 6–8 weeks after injection, tumors were dissected, embedded in paraffin, sectioned and stained with hematoxylin and eosin (H&E).

Mass spectrometry analysis of CL and monolysocardiolipin (MLCL)

Analysis of CL and MLCL was performed as described in Houtkooper et al. (2009). In brief, lipids were extracted from homogenized cells by single phase extraction and cardiolipin $(14:0)_4$ was added for internal standardization. Extracted lipids were analyzed in a high-performance liquid chromatography–mass spectrometry (HPLC–MS) system.

Determination of respiratory capacity

Oxygen consumption rate (OCR) and extra-cellular acidification rate (ECAR) of iPSCs were measured with a XF96 Extracellular Flux Analyzer (Seahorse Bioscience, Billerica, MA, USA). BTHS and control iPSCs were cultured onto growth factor-reduced matrigel-coated (matrigel^{GFR}, BD Biosciences) tissue culture dishes without feeder layer. Briefly, hiPSCs cultured on MEFs were digested with collagenase IV, scraped off gently with a cell scraper and cultured onto matrigel^{GFR}-coated plates in MEF-conditioned medium containing 10 ng/ml bFGF as described before (Pakzad et al., 2010). When hiPSCs reached confluence, a single cell suspension was obtained by the digestion of the cells with accutase. BTHS and control iPSCs were seeded to a density of 5×10^3 cells/well into a matrigel^{GFR}-coated XF 96-well cell culture microplate one day before measurements and cultured as a monolayer in MEF-conditioned medium containing 10 ng/ml bFGF. To increase the cell survival rate of dissociated iPSCs, 10 μM of Rho-associated kinase (ROCK) inhibitor Y-27632 was used 90 min before digestion with accutase (Pakzad et al., 2010). Baseline respiration was measured in unbuffered DMEM without bicarbonates supplemented with 1 mM pyruvate and 25 mM glucose after calibration at 37 °C in an incubator without CO_2. Periodic measurements of oxygen consumption and pH were performed and OCR and ECAR were calculated from the slopes of change in concentration in these parameters over time. Metabolic states were measured after subsequent addition of 1.5 μM oligomycin, 1 μM carbonyl cyanide 4-(trifluoromethoxy)phenylhydrazone (FCCP), 1 μM antimycin A, and 1 μM rotenone.

For analyzing the growth rate, a single cell suspension was seeded in the meanwhile at a density of 1×10^5 cells/well in 6-well plate. The cell number was calculated using a cell counting chamber at 24 h after cell seeding. Each sample was assayed in duplicates in 3 independent experiments.

Membrane potential measurement

Membrane potential measurements were performed in buffer MP (20 mM KPi, pH 7.2, 0.6 M sorbitol, 0.1% (w/v) bovine serum albumin, 10 mM $MgCl_2$, 0.5 mM EDTA, 20 mM succinate,

and 4 mM malate). The membrane potential ($\Delta\psi$) sensitive dye $DiSC_3(5)$ (3,3-dipropylthiadicarbocyanine iodide, Molecular Probes) was added to a final concentration of 1 μM. 100 μg/ml of isolated mitochondria was added and the specific fluorescence quenching was recorded using a spectrometer (F-7000, Hitachi) at an excitation wavelength of 622 nm, and an emission wavelength of 670 nm until a stable baseline was reached. To inhibit the respiratory chain 9 mM KCN was added and the dissipated membrane potential was recorded (Sims et al., 1974).

Blue native PAGE

Mitochondrial membranes were solubilized in 1% digitonin, 20 mM Tris–HCl, pH 7.4, 0.1 mM EDTA, 50 mM NaCl, 10% (w/v) glycerol, 1 mM PMSF for 30 min at 4 °C. After a clarifying spin for 15 min at 20,000 ×*g* and 4 °C, 10× loading dye (100 mM Bis-Tris pH 7.0, 5% Coomassie brilliant blue G-250, 500 mM ε-amino n-caproic acid) was added to the supernatant and the sample was separated on a 3–8% polyacrylamide gradient gel as described (Dekker et al., 1996).

Miscellaneous

Isolation of mitochondria from BTHS and control iPSCs was performed as described in (Lazarou et al., 2009). In brief, cells were homogenized in THE buffer (10 mM HEPES pH 7.4, 300 mM Trehalose, 10 mM KCl, 1 mM EDTA, 1 mM EGTA, and 0.5 mM PMSF) by mechanical disruption. After a clarifying spin at 400 ×*g* for 10 min at 4 °C mitochondria were harvested from the supernatant by centrifugation at 11,000 ×*g* for 5 min at 4 °C. ROS generation of isolated mitochondria was monitored using H_2DFFDA (Invitrogen). Changes of fluorescence of 10 μM H_2DDFDA in 250 μl assay buffer (20 mM Tris–HCl pH 7.4, 150 mM NaCl, and 1% Triton X-100) was recorded at an excitation wavelength of 498 nm and an emission wavelength of 525 nm using a fluorescence spectrophotometer (Hitachi F-7000) for 10 min. For analysis of mitochondrial protein content 100,000 cells were lysed in buffer L (50 mM Tris pH 7.4, 140 mM NaCl, 1 mM $MgCl_2$, 1% NP40, and 2 mM PMSF) by sonication. Cleared supernatants were normalized for protein content and subjected to SDS gel electrophoresis using standard techniques. Proteins were bound to polyvinylidene fluoride (PVDF) membranes by Western-blotting and probed using primary antibodies raised in rabbit and secondary antibodies coupled to horseradish peroxidase. Signals were detected using the ECL detection system (GE-Healthcare) and X-ray films.

Results

Generation and characterization of BTHS–iPSCs

Dermal fibroblasts were obtained from three male BTHS patients (TAZ10, TAZ13, and TAZ15) with different mutation sites in the *TAZ1* gene (590 G>T, 110-1 AG>AC, 170 G>T) (Houtkooper et al., 2009), and transduced with the STEMCCA lentiviral vector that contains *SOX2*, *KLF4*, *OCT4* and *c-MYC*, using the standardized protocol reported previously (Streckfuss-Bomeke et al., 2012). After 4 weeks of infection, a number of colonies with typical human ESC-like morphology were manually picked and expanded. At least three independent iPSC lines were generated and characterized from each patient (Table 1). Similarly, control iPSC lines were generated from one healthy individual (C113), which contains none of the mutations. All generated BTHS and control iPSCs showed typical human ESC morphology (Fig. 1A, Supplementary Figs. S1A–C). Each of iPSC lines has been maintained for more than 20 passages without any obvious phenotypic changes.

All generated BTHS and control iPSCs showed alkaline phosphatase activity (Fig. 1B, Supplementary Figs. S1D–F) and were positive for human ESC markers NANOG, SOX2, OCT4, LIN28, SSEA-4 and TRA-1-60 demonstrated by immunofluorescence staining (Figs. 1C–H, Supplementary Figs. S1D–F). Genomic sequencing confirmed that the generated BTHS–iPSC lines retained the specific mutation sites as in their parental fibroblasts (Fig. 1I). All mutations are hemizygous because the *TAZ1* gene is located on the X-chromosome and BTHS–iPSCs are generated from the male patients. In addition, all generated BTHS and control iPSCs revealed endogenous expression of several pluripotency marker genes such as *OCT4*, *SOX2*, *LIN28* and *NANOG* at a similar level to human ESCs by RT-PCR (Fig. 1J). We also analyzed the DNA methylation status of the *OCT4* and *NANOG* promoters in generated iPSCs. The *OCT4* and *NANOG* promoters were hypermethylated in the donor dermal fibroblasts and hypomethylated in the reprogrammed iPSC lines (Fig. 1K) confirming the reactivation of endogenous expression of these two pluripotency genes.

Pluripotency of each iPSC line was assessed by both in vitro and in vivo differentiation potentials. Upon spontaneous differentiation via embryoid body formation, the generated iPSCs were able to differentiate into cells derived from all three embryonic germ layers in vitro, as detected by expression of marker proteins specific for mesoderm, smooth muscle α-actin (α-SMA), for endoderm, α-fetoprotein (AFP) and for ectoderm, β-III tubulin (Figs. 2A–C, Supplementary Fig. S2). When the generated iPSCs were subcutaneously injected into immunodeficient mice, teratoma formation was observed from all analyzed iPSC lines. The tumors contained abundant differentiation of advanced derivatives of three embryonic germ layers (Figs. 2D–F). Thus, these analyses confirmed that the generated BTHS and control iPSCs are pluripotent.

Impaired CL remodeling in BTHS–iPSCs

The characteristic abnormalities of CL remodeling in BTHS patients have been suggested as a diagnostic tool for the analysis of BTHS patients (Kulik et al., 2008). To confirm the generated iPSCs as a model for BTHS, we analyzed the CL and MLCL contents in a selected set of iPSCs by mass spectrometry (Fig. 3). Compared to control iPSCs C113, BTHS–iPSCs TAZ10 and TAZ13 displayed the typical defects in CL remodeling: lower CL levels, accumulation of MLCL, and a shift of CL and MLCL towards more saturated species. In C113 iPSCs, MLCL was hardly detectable, whereas in TAZ10 and TAZ13 iPSCs MLCL levels were markedly elevated. For both TAZ10 and TAZ13 cells CL levels were reduced when compared to C113. In addition, there was a shift towards higher m/z values for both MLCL and CL in TAZ10 and TAZ13

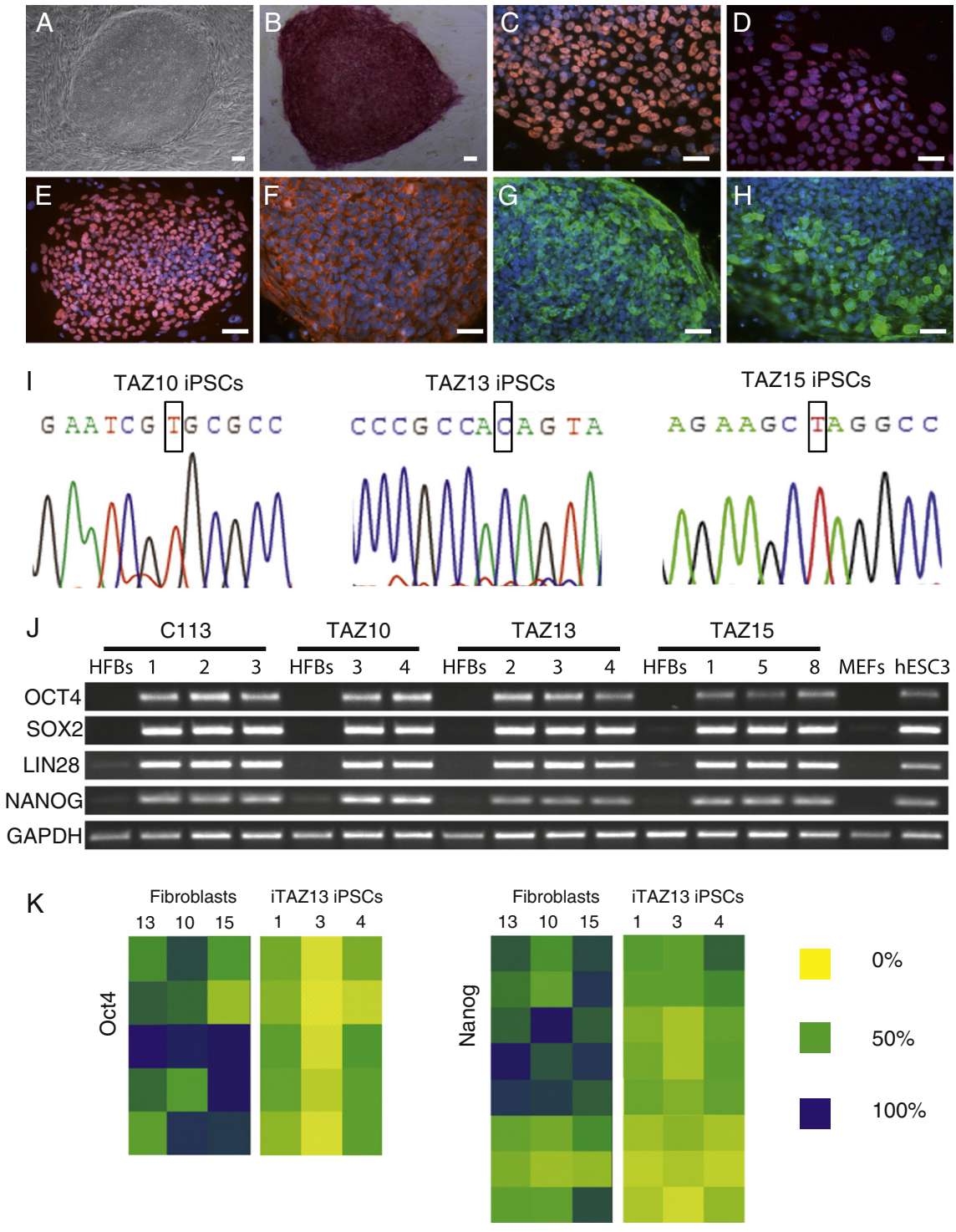

Figure 1 Characterization of patient-specific iPSCs. A. A representative human ESC-like colony of established TAZ15 iPSC line was shown. B. The TAZ15 iPSC colony expresses alkaline phosphatase activity. Scale bar = 50 μm. C–E. Immunocytochemical staining of TAZ15 iPSCs at passage 8 revealed NANOG, SOX2, and OCT4 expression at nuclei. F. LIN28 expression was abundant in the cytoplasm. G–H. The expression of SSEA-4 and TRA-1-60 was detected in the plasma membrane. Nuclei were stained with DAPI. Scale bar = 50 μm. I. The results of genomic sequence analysis show the existence of the mutation site in the generated iPSCs. J. RT-PCR analyses show that the iPSCs express pluripotency markers. Untransduced human fibroblasts (HFBs) and MEFs served as a negative control and human ESCs used as positive control. K. DNA methylation of *OCT4* and *NANOG* promoter regions was examined by bisulfite genomic sequencing and compared between untransduced fibroblast from 3 patients and generated iPSCs. Color codes from 0% (yellow), over 50% (green) to 100% (blue) methylation.

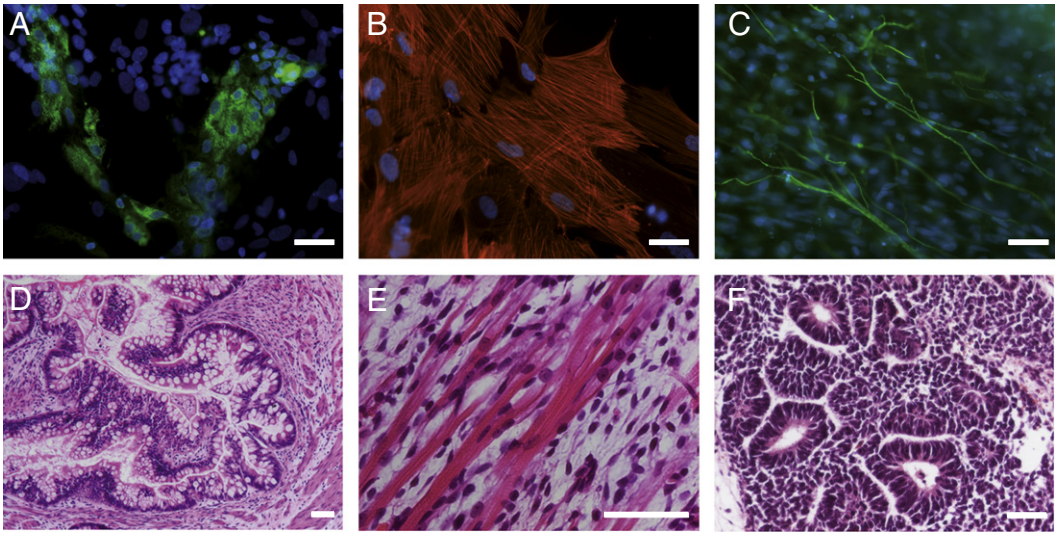

Figure 2 Patient-specific iPSCs are pluripotent. A–C. Immunocytochemical staining of embryoid body-mediated differentiated TAZ15 iPSCs at day 8 + 25 revealed expression of α-fetoprotein (A), α-smooth muscle actin (B) and βIII-tubulin (C). Nuclei were stained with DAPI. Scale bar = 50 μm. D–F. Upon subcutaneous injection of undifferentiated iPSCs into RAG2$^{-/-}\gamma c^{-/-}$ immunodeficient mice, teratoma was formed after 6–8 weeks. The teratoma contains derivatives of all three germ layers, epithelium (endoderm, D), muscle structure (mesoderm, E) and neural tissue (ectoderm, F). Scale bar = 50 μm.

iPSCs reflecting the higher degree of saturation of the fatty acid side chains (compare highest peaks of different CL clusters; i.e. the peak at m/z = 699.5 in C113 is shifted to m/z = 701.5 in TAZ10 and TAZ13 and the peak at m/z = 712.5 is shifted to m/z = 714.5 etc.).

BTHS–iPSCs display decreased respiration not compensated by increased glycolysis

To address the molecular pathology of the BTHS–iPSC model, we analyzed mitochondrial respiration in iPSC derived from control individuals and BTHS patients. In order to submit iPSCs to flourescense based oxygen consumption measurement, iPSCs were digested into single cells and cultured as a monolayer under feeder-layer free conditions one day before the measurements as described in the Material and methods. The change in concentration of molecular oxygen over time (oxygen consumption rate, OCR) under basal conditions was first measured for three independent iPSC lines derived from fibroblasts of patient TAZ15 and three control iPSC lines (Fig. 4A). We calculated an average OCR of all three BTHS–iPSC lines and found a significant reduction to 62% of the basal respiration (Fig. 4B). In the same measurement, we inhibited the F_1F_O ATP-synthase by using the specific inhibitor oligomycin. The decrease of respiration in control and patient lines is a result of the tight coupling between the respiratory chain and the F_1F_O ATP-synthase by the membrane potential. Subsequent depolarization of the membrane potential with FCCP uncouples the respiratory chain from the ATP-synthase and reveals the maximal respiratory capacity, which is significantly reduced in BTHS–iPSCs (Fig. 4A). A block of complexes I and III with rotenone and antimycin A, respectively, completely inhibits mitochondrial respiration and therefore reveals non-mitochondrial O_2 consumption of the cell. The maximum respiratory capacity, defined as the difference of FCCP uncoupled respiration and residual non-mitochondrial respiration ($OCR^{FCCP} - OCR^{ROTENONE}$), was reduced in BTHS–iPSCs (TAZ15) to 53% of control iPSCs (C113) (Fig. 4C). For these assays cells were plated at a concentration of 5×10^3 cells/well one day prior to the measurement. To confirm that a difference in the growth rates of BTHS and control cells did account for differences in respiration, we determined cell numbers prior to the measurements and did not observe significant growth differences among iPSC lines used (Supplementary Fig. 3A). To exclude that the observed decreased respiration in BTHS–iPSCs was caused by decreased mitochondrial content instead of a specific defect in the respiratory chain function, we analyzed the mitochondrial protein content of a normalized amount of cells by Western blot. Our data showed that mitochondrial protein levels were comparable in BTHS and control iPSCs (Supplementary Fig. 3B).

Glycolysis allows cells to generate ATP by metabolizing glucose to lactate in the absence of oxidative phosphorylation. As lactate is excreted from the cell, the change of pH over time in an unbuffered medium (extracellular acidification rate, ECAR) was assessed to determine the glycolytic rate. We measured ECAR simultaneously while recording OCR for three TAZ15 iPSC lines in comparison to three control iPSC lines. The rate of glycolysis immediately increases after the block of respiration with oligomycin, which was reverted after uncoupling with FCCP. Surprisingly, glycolysis in BTHS–iPSCs was not upregulated to compensate for the decreased respiration. The ratio of OCR/ECAR indicates the relative contribution of mitochondrial respiration and glycolysis to the total energy consumption. Fig. 4D shows a comparable OCR/ECAR ratio in control and patient iPSCs under all conditions indicating that despite severely reduced respiration in patient iPSCs, glycolysis is unable to compensate for this defect.

To assess if the observed respiratory deficiency was a general characteristic of BTHS patients, we analyzed the

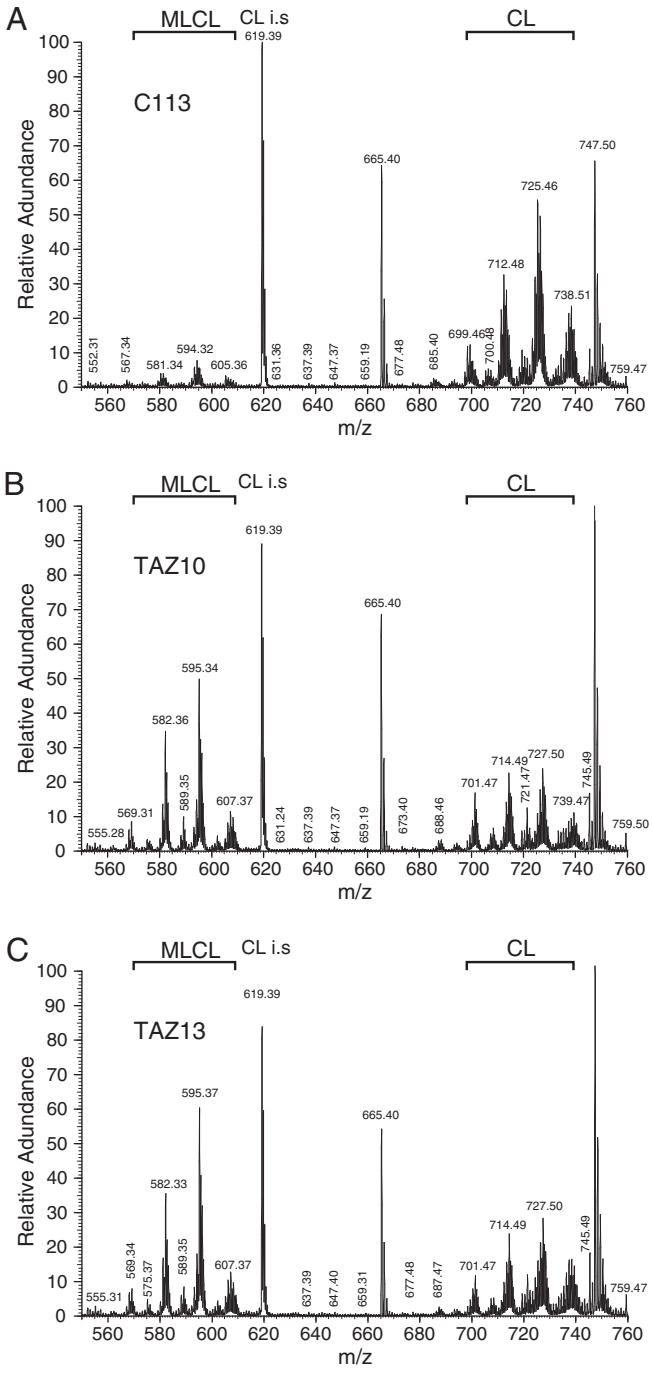

Figure 3 Cardiolipin remodeling is strongly affected in BTHS–iPSCs. Mass spectrometry analysis of cardolipin (CL) and monolysocardiolipin (MLCL) contents in C113 control (A) and BTHS TAZ10 (B) and TAZ13 (C) iPSCs. Spectrum is presented as mass to charge ratio (m/z). Cardiolipin $(14:0)_4$ m/z 619.5 served as an internal standard (i.s.).

respiration of iPSC lines generated from two other patients, TAZ10 and TAZ13. We included control iPSCs generated previously from two other healthy individuals (WT-D2, WT-K1) (Streckfuss-Bomeke et al., 2012). The basal OCR of two iPSC lines of TAZ10 and healthy individuals was measured, and subsequently oligomycin inhibited respiration and maximal respiratory capacity after addition of FCCP was determined (Fig. 5A). Basal respiration of TAZ10 iPSCs was strongly affected when compared to control cells (36% of control, Fig. 5B). Patient iPSCs hardly responded to addition of oligomycin and uncoupling using FCCP (Fig. 5A). We simultaneously measured ECAR of TAZ10 iPSCs during the experiment in order to determine the rate of glycolysis. OCR/ECAR ratio in TAZ10 iPSCs was slightly reduced indicating that the mitochondrial contribution to energy conversion in patient TAZ10 was lower compared to the control individual, however glycolysis was insufficient to compensate for the reduced respiration (Fig. 5C). The measurement of basal respiration, oligomycin inhibited respiration and FCCP uncoupled respiration of TAZ13 iPSCs is depicted in Fig. 5D.

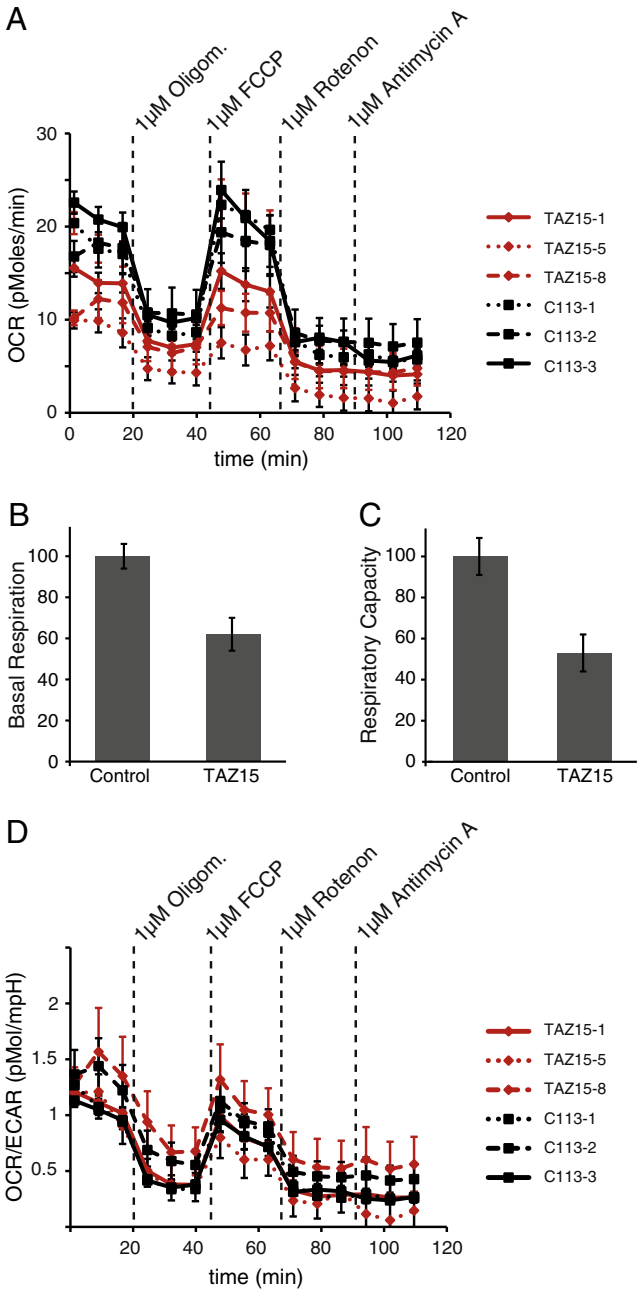

Figure 4 Deficient respiration of hiPSCs derived from Barth syndrome patient TAZ15 is not compensated by glycolysis. A. Oxygen consumption rate (OCR) of three control hiPSC lines and three hiPSC lines derived from Barth syndrome patient TAZ15. After periodic measurement of the basal respiration the indicated compounds were subsequently added and the OCR rate was determined. B. For calculation of basal OCR, averages of all three hiPSC lines derived from patient TAZ15 before compound administration was compared to control (set to 100%). C. The maximal respiratory capacity is calculated from the average respiration of three iPSC lines after FCCP administration minus the average of non-mitochondrial O_2 consumption after Rotenone treatment (control set to 100%). D. Extracellular acidification rate (ECAR) was measured simultaneously to OCR and plotted as the ratio OCR/ECAR indicating metabolic shifting of the cells.

Basal OCR of TAZ13 iPSCs, carrying a splice acceptor mutation, was even more affected than other patients and reduced to 32% of control cells (Fig. 5E). The FCCP uncoupled maximal respiration was affected to a similar extent.

The membrane potential across the inner membrane is essential for almost all transport processes across the inner membrane of mitochondria. We hypothesized that the respiratory deficiency in BTHS–iPSCs would result in a decreased proton pumping activity and a measurable reduction of the membrane potential. We isolated mitochondria from control, TAZ10 and TAZ15 iPSCs and used these to measure the membrane potential by fluorescence quenching

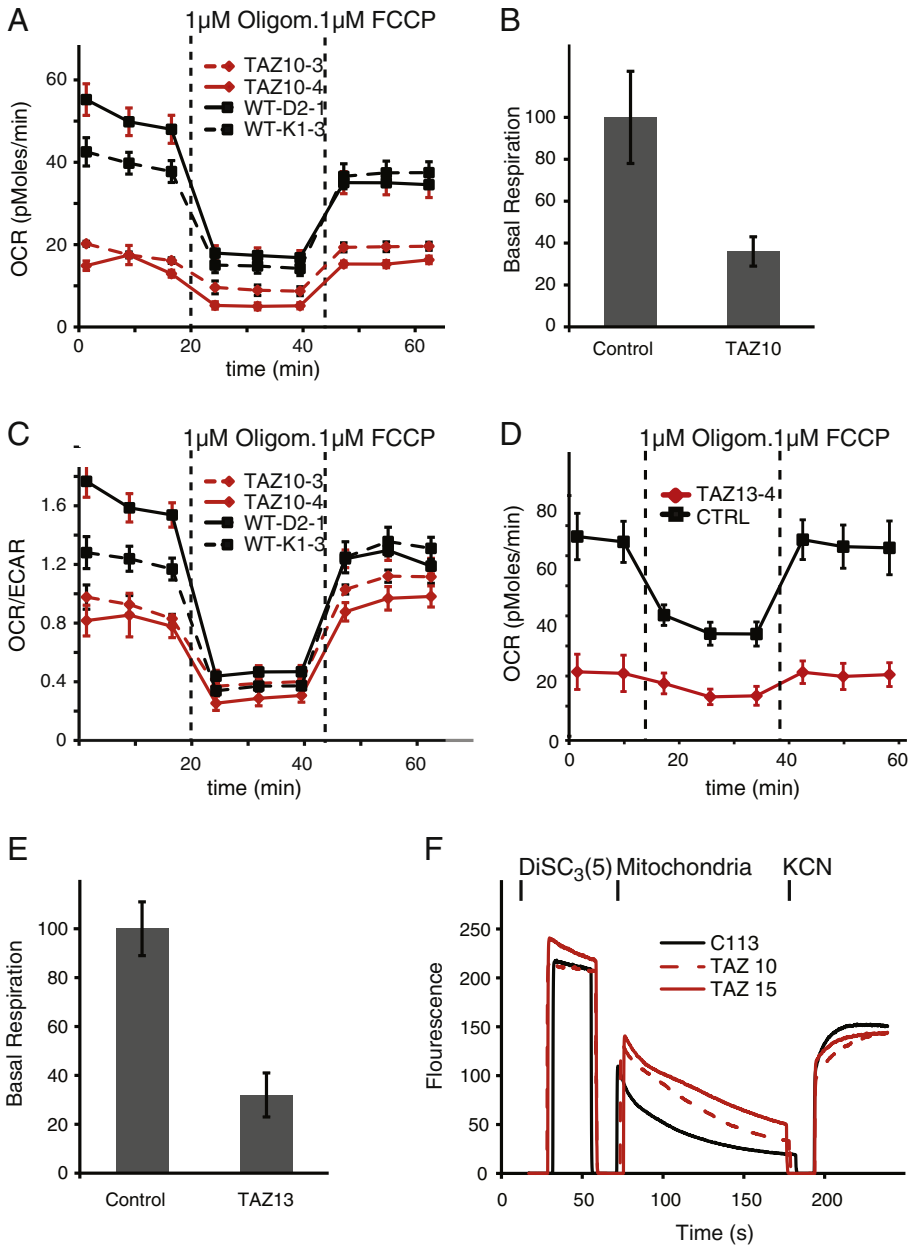

Figure 5 Inefficient respiration in Barth syndrome iPSCs results in a decreased membrane potential. A. Periodic measurement of OCR rates of two control and two patient (TAZ10) iPSC lines before and after administration of the indicated compounds. B. Quantification of the average basal respiration of two TAZ10 iPSC lines measured in A compared to control cells (set to 100%). C. Simultaneous measurement of ECAR allows the determination of OCR/ECAR ratios. D. Determination of OCR in patient TAZ13 iPSCs compared to control. E. Quantification of the basal respiration of patient TAZ13 iPSCs compared to control (set to 100%). F. Membrane potential of isolated mitochondria of iPSCs derived from control and Barth syndrome patients TAZ10 and TAZ15 is determined by fluorescence quenching of the $\Delta\psi$ dependent dye $DiSC_3(5)$. Membrane potential specific decrease of fluorescence is determined by intoxication of complex IV using KCN. One representative reading is shown.

utilizing the membrane potential-sensitive dye $DiSC_3(5)$. As expected, while a strong quenching of fluorescence was observed in control iPSC mitochondria after dye administration, mitochondria from BTHS–iPSCs showed a strongly reduced quenching efficiency, demonstrating a decreased membrane potential (Fig. 5F). Taken together, these data show that cardiolipin deficiency in the BTHS–iPSC model system strongly affects mitochondrial respiration resulting in a decreased membrane potential.

Respiratory chain complexes are reorganized in BTHS–iPSCs

For efficient energy transfer, respiratory chain complexes are organized into large oligomers in the inner membrane, referred to as supercomplexes. In human mitochondria, supercomplexes are formed by complex I, which builds a platform for binding of dimeric complex III and several copies of complex IV (Schägger and Pfeiffer, 2001; Moreno-Lastres et

al., 2012). The strong deficiency in respiration in BTHS–iPSC triggered our interest in the structural organization of respiratory chain complexes in these patient cells. To address this question and determine if the analysis of respiratory chain complexes from control and patient iPSCs was feasible, we isolated mitochondria from iPSCs TAZ10, TAZ13, TAZ15 and controls for biochemical analyses. As the cultivation of stem cells required the presence of a limited amount of MEFs, a mock isolation of a comparable amount of feeder cell was performed in parallel. Using the mild detergent digitonin, we solubilized membranes of isolated mitochondria and separated membrane protein complexes by Blue-native gel electrophoresis. For Western blot analysis we used specific antibodies against components of the respiratory chain: NDUFB8 (complex I), RIESKE (complex III), and COX5A and COX6A (complex IV). All four antibodies detected supercomplexes in the high molecular weight range in control iPSCs (Fig. 6A). However, these supercomplexes were strongly reduced or absent in TAZ13 iPSCs. In contrast, amounts of smaller complexes were increased in TAZ13 iPSCs compared to control cells. This was especially noticeable for the heterooligomeric complexes III_2–IV, the dimeric complex III_2 and monomeric complex IV. A slightly faster migration behavior of these complexes in TAZ13 iPSCs either indicates a different solubilization due to the lack of cardiolipin or a loss of single components during the preparation of the samples. A significant detection in mock isolated MEF mitochondria was only observed, when highly overexposed, confirming the specificity of the signal for hiPSC mitochondria (Fig. 6A).

To understand if structural rearrangements were common to BTHS patients we analyzed mitochondria isolated from TAZ10 and TAZ15 iPSCs by BN-PAGE (Fig. 6B). Similar to what was observed for TAZ13 iPSCs, supercomplexes were strongly reduced or absent in iPSCs of both patients. TAZ15 iPSCs showed an increase of the complexes III_2–IV and complex III_2, similar to TAZ13. However, in TAZ10 iPSCs, the smaller complexes III_2–IV and III_2 were present in reduced amounts, indicating a reduced stability of both complexes. In order to assess protein stability of patient TAZ10 and TAZ15 iPSCs we analyzed steady state levels of isolated mitochondria by SDS gel electrophoresis and subsequent Western-blotting. Mitochondrial proteins were detected in comparable amounts in all samples (Fig. 6C). Only a slight decrease of COX5A in both patients' iPSCs and COX6A in TAZ10 compared to control cells became apparent. Thus, we conclude that a lack of cardiolipin in the BTHS–iPSC model respirasome formation is significantly affected.

Structural reorganization of the respiratory chain is often associated with less efficient energy coupling and the generation of reactive oxygen species (ROS). We therefore asked if due to respirasome reorganization and potential malfunction in electron transfer ROS production was increased in patient iPSCs. Therefore, we measured ROS in isolated mitochondria from control and TAZ13 iPSCs using the fluorescence-based sensor H_2DFFDA. Interestingly, mitochondria from Barth syndrome patient TAZ13 showed a significant increase in ROS generation compared to control cells (Fig. 6D). Accordingly, dissociation of respirasomes in BTHS patient iPSCs coincided with an increase in the production of reactive oxygen species.

Discussion

We have developed the first human iPSC-based model for BTHS, bearing mutations in *TAZ1*, and demonstrated its suitability to recapitulate mitochondrial dysfunction of the disease phenotype. So far, insight into the pathogenesis of BTHS has been gained primarily from patient derived fibroblasts and lymphoblasts and a mouse tafazzin knock down model. BTHS patient fibroblasts and lymphoblasts have defined the characteristic abnormalities in CL remodeling and have helped to understand the role of cardiolipin in shaping mitochondrial morphology and maintaining the integrity of the respiratory chain (Xu et al., 2005; Acehan et al., 2007; Mckenzie et al., 2006; Barth et al., 1996). Recently, the systemic knock down of tafazzin in a mouse model was described. However, the late onset of clinical symptoms triggers questions how well the mouse model recapitulates the situation in human tissue (Acehan et al., 2011; Soustek et al., 2011), in particular, since recent research focused on BTHS as a multi-organ disorder, which has a significant impact on fetal and perinatal male demise, stillbirth and severe neonatal illness or death (Steward et al., 2010).

In this study we used dermal fibroblasts derived from three different patients with distinct mutations in the *TAZ1* gene (Houtkooper et al., 2009) and generated BTHS patient-specific iPSCs. We fully characterized them in terms of pluripotency both in vitro and in vivo. Similar to human ESCs, all generated iPSCs show the self-renewal capacity and are able to differentiate into derivatives of all three embryonic germ layers. Importantly, BTHS–iPSCs exhibit the typical defects in CL remodeling: lower CL levels, accumulation of MLCL, and a shift of CL and MLCL towards more saturated species. It is important to note that the CL composition of cultured iPSCs differs from the CL composition in heart tissue, in which tetralinoleyl-CL is the predominant form (Houtkooper et al., 2009). Cultured iPSCs contained the main CL clusters found in heart, but the linoleic acid content is lower. One likely explanation is that cultured iPSCs rely predominantly on glucose as their major source of energy (in contrast to the heart); therefore, the CL composition in iPSCs does not need specific adaptation to tetralinoleyl-CL for optimizing high mitochondrial activity. Similar hypothesis has been suggested for the CL composition in the brain by Cheng et al. (2008). Another likely explanation is that the lipid composition in cultured cells highly depends on the fatty acids available in the culture medium. A direct correlation of CL fatty acid composition and fatty acid supplementation in the growth media has been shown previously for patient fibroblasts (Valianpour et al., 2003). Further studies should investigate the CL composition in cultured cardiomyocytes derived from iPSCs.

In our iPSC model of BTHS, we observed structural rearrangements of respiratory chain complexes in all iPSC lines derived from three different patients, which most dramatically affect the large supercomplexes (respirasomes) (Figs. 6A and B), consistent with data from Barth patient derived lymphoblasts (Mckenzie et al., 2006). In these studies, the I–III_2 complexes was the largest respiratory complex which was stable in Barth patients. This form is hardly visible in Figs. 6A and B, however, extended exposures confirmed it to be stable in BTHS patient iPSCs (data not

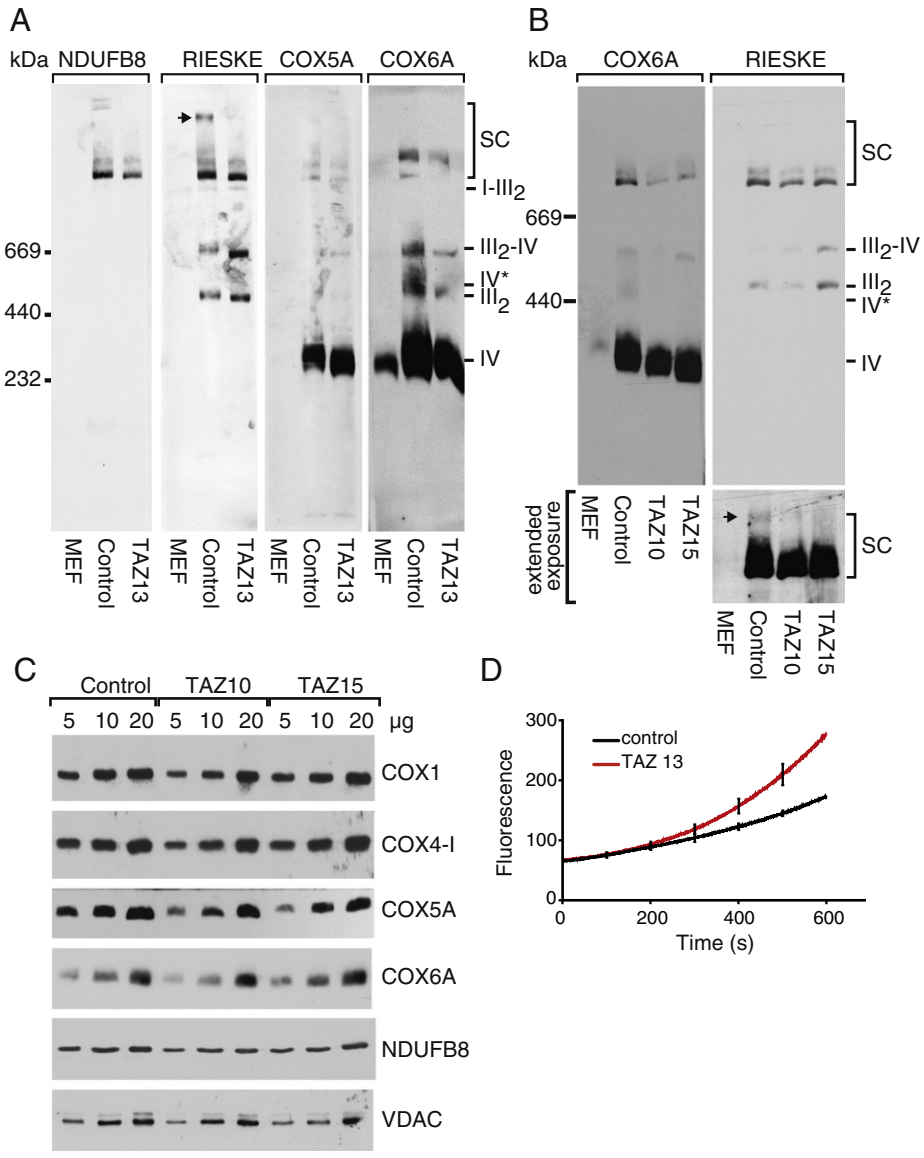

Figure 6 Rearrangements of mitochondrial respiratory chain supercomplexes in Barth syndrome iPSCs cause inefficient energy transfer resulting in increased generation of ROS. A and B. Isolated mitochondria from patient and control iPSCs and MEFs as a control were solubilized in digitonin and analyzed on BN-PAGE. Respiratory chain complexes were visualized by Western blot detection using indicated antibodies. Arrowheads indicate the large supercomplex forms only present in control mitochondria C. Serial dilutions of mitochondrial extract were separated in SDS gel electrophoresis and analyzed in Western blot using the indicated antibodies. D. Measurement of ROS generation over time in isolated mitochondria from TAZ13 hiPSCs using the ROS-specific fluorescence-based sensor H_2DFFDA (arbitrary units).

shown). Steady state level protein analysis indicated that the stability of most constituents of the respiratory chain complexes is not affected (Fig. 6C). Instead, smaller assembly forms of respiratory chain complexes, such as the dimer of complex III_2, monomeric complex IV and the III_2–IV heterooligomer become more prominent in BTHS–iPSCs. Interestingly, these complexes showed a slightly faster migration behavior in TAZ13 iPSCs. The faster migration of the monomeric complex IV has been observed before in lymphoblast of Barth patients (Mckenzie et al., 2006) and can be either explained by differences in the solubilization of the complexes due to the absence of cardiolipin or by the dissociation of single components. Structural data revealed that components, such as COX6A form the periphery of the cytochrome *c* oxidase complex (Tsukihara et al., 1996) and biochemical data indicate that dissociation of peripheral subunits occurs with decreasing CL content (Sedlák and Robinson, 1999).

The formation of respiratory chain supercomplexes is essential for efficient energy transformation. To evaluate if the structural reorganization, observed in BTHS patients will affect mitochondrial respiration, we analyzed the metabolism of BTHS–iPSCs. Patient TAZ10 and TAZ13 iPSCs showed a strong defect in basal respiration as well as in their maximal

respiratory capacity, indicative of reduced energy conversion by the respiratory chain complexes. An assessment of cellular growth rate excluded the possibility that a difference in cell numbers is responsible for this effect. A determination of mitochondrial proteins of a normalized amount of cells also excluded the possibility that impaired respiration in these cells is a result of decreased mitochondrial proliferation. In line with our findings, previous reports showed that mitochondrial content in BTHS fibroblast and lymphoblast is rather increased than decreased (Xu et al., 2005; Barth et al., 1996). We therefore conclude that the structural remodeling of supercomplexes results in a decreased mitochondrial respiration, in agreement with earlier reports on a decreased activity of complexes III and IV (Xu et al., 2005; Barth et al., 1996). Interestingly, full uncoupling using FCCP induces respiratory rates comparable to basal respiration. This is in contrast to what has been observed for differentiated cells such as fibroblasts. We speculate that basal respiration of iPSCs is close to maximal respiration and decreases after initiation of differentiation. We propose that the mutation in TAZ13 in a splice acceptor site at the intron 1–exon 2 boundary will result in a non-functional form of the tafazzin protein, explaining the severity of this mutant. Patient TAZ15 shows a slightly milder phenotype in respiratory measurements. Recently, a yeast mutant resembling the mutation of Barth patient TAZ15 was described (Whited et al., 2012). The yeast mutant protein was stable and localized in the IMS within mitochondria. When the enzymatic transacylase activity was determined, only prolonged exposure to restrictive conditions decreased enzymatic activity, indicative of a temperature sensitive phenotype of this mutant. We therefore conclude that differences in the severity of the mutation might be reflected in the extent of respiratory deficiency. Clinically, the severity of manifestations of BTHS varies among patients. Larger sets of BTHS–iPSC lines harboring different mutations in *TAZ1* are therefore valuable to further validate the patient-specific and mutation site-specific disease phenotype and compare pathogenetic mechanisms in diverse forms of the disease.

In agreement with the idea that supercomplex formation promotes efficient energy transduction, measurement of the proton pumping activity in BTHS–iPSCs showed a strong reduction of the membrane potential in the two patients analyzed. A reduced membrane potential was also detected in lymphoblasts from BTHS patients (Xu et al., 2005), but normal levels of cellular ATP was measured in patient fibroblasts, which may be due to the increase in mitochondrial mass (Xu et al., 2005; Barth et al., 1996). Our analyses further show that the destabilization of supercomplexes results in a leakage of electrons and thus enhanced generation of ROS. In support of this observation a yeast model for BTHS, the *taz1*Δ strain, displayed accumulation of ROS (Chen et al., 2008). Complex III is predominantly involved in ROS generation in mitochondria. Cardiolipin deficiency was shown to cause structural changes in this complex, affecting the heme centers which might lower the driving force of electron transfer and provokes ROS generation (Wenz et al., 2009).

Our data provide clear evidence that the pathogenesis of the *TAZ1* mutations can be modeled in iPSCs derived from patients with BTHS. Since BTHS is multisystem disorders, characterized by dilated cardiomyopathy, attended with skeletal myopathy and neutropenia (Barth et al., 1983; Spencer et al., 2005; Takeda et al., 2011), the iPSC approach is particularly attractive due to the pluripotent nature of these cells. Future studies will have to differentiate BTHS–iPSCs into cardiomyocytes, skeletal muscle cells and other cell types and to assess the mitochondrial and bioenergetic changes in these cell lineages. It will be important to study whether both, increased ROS generation and reduced energy supply caused by inefficient respiration, contribute to the pathogenesis in the heart or other tissues of BTHS patients. The generation of ROS has been implicated in a variety of cardiovascular diseases (Dhalla et al., 2000; Ytrehus et al., 1987). The potentially unlimited number of induced organ-specific cells will allow us to investigate the molecular and pathophysiological mechanisms and to establish high-throughput drug screening.

Conclusion

In summary, we generated iPSCs from patients with BTHS. As compared with iPSCs derived in a similar fashion from healthy controls, BTHS–iPSCs exhibited an impaired CL remodeling, an altered mitochondrial oxygen consumption, which is not compensated by increased glycolysis, and an increased generation of ROS, thus demonstrating that iPSC models recapitulate the phenotypes of the disease.

Acknowledgments

We thank Anke Cierpka, Yvonne Hintz, Sandra Georgi, and Yvonne Wiegeräfe for excellent technical assistance. This work was supported by the Deutsche Forschungsgemeinschaft, SFB 1002 (PR and KG), by Bundesministerium für Bildung und Forschung grant 01GS0837 (KG), and the Max Planck Society (PR).

Appendix A. Supplementary data

Supplementary data to this article can be found online at http://dx.doi.org/10.1016/j.scr.2013.05.005.

References

Acehan, D., Xu, Y., Stokes, D.L., Schlame, M., 2007. Comparison of lymphoblast mitochondria from normal subjects and patients with Barth syndrome using electron microscopic tomography. Lab. Invest. 87, 40–48.

Acehan, D., Vaz, F., Houtkooper, R.H., James, J., Moore, V., Tokunaga, C., Kulik, W., Wansapura, J., Toth, M.J., Strauss, A., Khuchua, Z., 2011. Cardiac and skeletal muscle defects in a mouse model of human Barth syndrome. J. Biol. Chem. 286, 899–908.

Acín-Pérez, R., Fernández-Silva, P., Peleato, M.L., Pérez-Martos, A., Enriquez, J.A., 2008. Respiratory active mitochondrial supercomplexes. Mol. Cell. 32, 529–539.

Arnaudo, E., Hirano, M., Seelan, R.S., Milatovich, A., Hsieh, C.L., Fabrizi, G.M., Grossman, L.I., Francke, U., Schon, E.A., 1992. Tissue-specific expression and chromosome assignment of genes specifying two isoforms of subunit VIIa of human cytochrome c oxidase. Gene 119, 299–305.

Bachman, N.J., Riggs, P.K., Siddiqui, N., Makris, G.J., Womack, J.E., Lomax, M.I., 1997. Structure of the human gene (COX6A2)

for the heart/muscle isoform of cytochrome c oxidase subunit VIa and its chromosomal location in humans, mice, and cattle. Genomics 42, 146–151.

Barth, P., Scholte, H., Berden, J., Van der Klei-Van Moorsel, J., Luyt-Houwen, I., Van't Veer-Korthof, E., Van der Harten, J., Sobotka-Plojhar, M., 1983. An X-linked mitochondrial disease affecting cardiac muscle, skeletal muscle and neutrophil leucocytes. J. Neurol. Sci. 62, 327–355.

Barth, P., Van den Bogert, C., Bolhuis, P., Scholte, H., van Gennip, A., Schutgens, R., Ketel, A., 1996. X-linked cardioskeletal myopathy and neutropenia (Barth syndrome): respiratory-chain abnormalities in cultured fibroblasts. J. Inherit. Metab. Dis. 19, 157–160.

Bazán, S., Mileykovskaya, E., Mallampalli, V.K.P.S., Heacock, P., Sparagna, G.C., Dowhan, W., 2012. Cardiolipin-dependent reconstitution of respiratory supercomplexes from purified *Saccharomyces cerevisiae* complexes III and IV. J. Biol. Chem.

Brandner, K., Mick, D., Frazier, A., Taylor, R., Meisinger, C., Rehling, P., 2005. Taz1, an outer mitochondrial membrane protein, affects stability and assembly of inner membrane protein complexes: implications for Barth Syndrome. Mol. Biol. Cell 16, 5202–5214.

Chen, S., He, Q., Greenberg, M.L., 2008. Loss of tafazzin in yeast leads to increased oxidative stress during respiratory growth. Mol. Microbiol. 68, 1061–1072.

Chen, Y.-C., Taylor, E.B., Dephoure, N., Heo, J.-M., Tonhato, A., Papandreou, I., Nath, N., Denko, N.C., Gygi, S.P., Rutter, J., 2012. Identification of a protein mediating respiratory supercomplex stability. Cell Metab. 15, 348–360.

Cheng, H., Mancuso, D.J., Jiang, X., Guan, S., Yang, J., Yang, K., Sun, G., Gross, R.W., Han, X., 2008. Shotgun lipidomics reveals the temporally dependent, highly diversified cardiolipin profile in the mammalian brain: temporally coordinated postnatal diversification of cardiolipin molecular species with neuronal remodeling. Biochemistry 47, 5869–5880.

Dekker, P., Müller, H., Rassow, J., Pfanner, N., 1996. Characterization of the preprotein translocase of the outer mitochondrial membrane by blue native electrophoresis. Biol. Chem. 377, 535–538.

Dhalla, N.S., Temsah, R.M., Netticadan, T., 2000. Role of oxidative stress in cardiovascular diseases. J. Hypertens. 18, 655–673.

Gebert, N., Joshi, A.S., Kutik, S., Becker, T., Mckenzie, M., Guan, X.L., Mooga, V.P., Stroud, D.A., Kulkarni, G., Wenk, M.R., Rehling, P., Meisinger, C., Ryan, M.T., Wiedemann, N., Greenberg, M.L., Pfanner, N., 2009. Mitochondrial cardiolipin involved in outer-membrane protein biogenesis: implications for Barth syndrome. Curr. Biol. 19, 2133–2139.

Grossman, L.I., Lomax, M.I., 1997. Nuclear genes for cytochrome c oxidase. Biochim. Biophys. Acta 1352, 174–192.

Houtkooper, R.H., Turkenburg, M., Poll-The, B.T., Karall, D., Perez-Cerda, C., Morrone, A., Malvagia, S., Wanders, R.J., Kulik, W., Vaz, F.M., 2009. The enigmatic role of tafazzin in cardiolipin metabolism. Biochim. Biophys. Acta 1788, 2003–2014.

Kulik, W., van Lenthe, H., Stet, F.S., Houtkooper, R.H., Kemp, H., Stone, J.E., Steward, C.G., Wanders, R.J., Vaz, F.M., 2008. Bloodspot assay using HPLC–tandem mass spectrometry for detection of Barth syndrome. Clin. Chem. 54, 371–378.

Lange, C., Nett, J.H., Trumpower, B.L., Hunte, C., 2001. Specific roles of protein–phospholipid interactions in the yeast cytochrome bc1 complex structure. EMBO J. 20, 6591–6600.

Lazarou, M., Smith, S.M., Thorburn, D.R., Ryan, M.T., Mckenzie, M., 2009. Assembly of nuclear DNA-encoded subunits into mitochondrial complex IV, and their preferential integration into supercomplex forms in patient mitochondria. FEBS J. 276, 6701–6713.

Lomax, M.I., Riggs, P.K., Womack, J.E., 1995. Structure and chromosomal location of the bovine gene for the heart muscle isoform of cytochrome c oxidase subunit VIII. Mammalian genome: official. J. Int. Mamm. Genome 6, 118–122.

Mckenzie, M., Lazarou, M., Thorburn, D.R., Ryan, M.T., 2006. Mitochondrial respiratory chain supercomplexes are destabilized in Barth Syndrome patients. J. Mol. Biol. 361, 462–469.

Moreno-Lastres, D., Fontanesi, F., García-Consuegra, I., Martín, M.A., Arenas, J., Barrientos, A., Ugalde, C., 2012. Mitochondrial complex I plays an essential role in human respirasome assembly. Cell Metab. 15, 324–335.

Neuwald, A., 1997. Barth syndrome may be due to an acyltransferase deficiency. Curr. Biol. 7, R465-R466.

Pakzad, M., Totonchi, M., Taei, A., Seifinejad, A., Hassani, S.N., Baharvand, H., 2010. Presence of a ROCK inhibitor in extracellular matrix supports more undifferentiated growth of feeder-free human embryonic and induced pluripotent stem cells upon passaging. Stem Cell Rev. 6, 96–107.

Pebay-Peyroula, E., Dahout-Gonzalez, C., Kahn, R., Trézéguet, V., Lauquin, G.J.-M., Brandolin, G., 2003. Structure of mitochondrial ADP/ATP carrier in complex with carboxyatractyloside. Nature 426, 39–44.

Pfeiffer, K., Gohil, V., Stuart, R., Hunte, C., Brandt, U., Greenberg, M., Schägger, H., 2003. Cardiolipin stabilizes respiratory chain supercomplexes. J. Biol. Chem. 278, 52873–52880.

Phoon, C.K.L., Acehan, D., Schlame, M., Stokes, D.L., Edelman-Novemsky, I., Yu, D., Xu, Y., Viswanathan, N., Ren, M., 2012. Tafazzin knockdown in mice leads to a developmental cardiomyopathy with early diastolic dysfunction preceding myocardial noncompaction. J Am Heart Assoc 1.

Robinton, D.A., Daley, G.Q., 2012. The promise of induced pluripotent stem cells in research and therapy. Nature 481, 295–305.

Schägger, H., Pfeiffer, K., 2000. Supercomplexes in the respiratory chains of yeast and mammalian mitochondria. EMBO J. 19, 1777–1783.

Schägger, H., Pfeiffer, K., 2001. The ratio of oxidative phosphorylation complexes I–V in bovine heart mitochondria and the composition of respiratory chain supercomplexes. J. Biol. Chem. 276, 37861–37867.

Schlame, M., Towbin, J.A., Heerdt, P.M., Jehle, R., DiMauro, S., Blanck, T.J.J., 2002. Deficiency of tetralinoleoyl-cardiolipin in Barth syndrome. Ann. Neurol. 51, 634–637.

Schlame, M., Kelley, R.I., Feigenbaum, A., Towbin, J.A., Heerdt, P.M., Schieble, T., Wanders, R.J.A., DiMauro, S., Blanck, T.J.J., 2003. Phospholipid abnormalities in children with Barth syndrome. J. Am. Coll. Cardiol. 42, 1994–1999.

Schwall, C.T., Greenwood, V.L., Alder, N.N., 2012. The stability and activity of respiratory complex II is cardiolipin-dependent. Biochim. Biophys. Acta 1817, 1588–1596.

Sedlák, E., Robinson, N.C., 1999. Phospholipase A(2) digestion of cardiolipin bound to bovine cytochrome c oxidase alters both activity and quaternary structure. Biochemistry 38, 14966–14972.

Shinzawa-Itoh, K., Aoyama, H., Muramoto, K., Terada, H., Kurauchi, T., Tadehara, Y., Yamasaki, A., Sugimura, T., Kurono, S., Tsujimoto, K., Mizushima, T., Yamashita, E., Tsukihara, T., Yoshikawa, S., 2007. Structures and physiological roles of 13 integral lipids of bovine heart cytochrome c oxidase. EMBO J. 26, 1713–1725.

Sims, P., Waggoner, A., Wang, C., Hoffman, J., 1974. Studies on the mechanism by which cyanine dyes measure membrane potential in red blood cells and phosphatidylcholine vesicles. Biochemistry 13, 3315–3330.

Soustek, M.S., Falk, D.J., Mah, C.S., Toth, M.J., Schlame, M., Lewin, A.S., Byrne, B.J., 2011. Characterization of a transgenic short hairpin RNA-induced murine model of tafazzin deficiency. Hum. Gene Ther. 22, 865–871.

Spencer, C.T., Byrne, B.J., Gewitz, M.H., Wechsler, S.B., Kao, A.C., Gerstenfeld, E.P., Merliss, A.D., Carboni, M.P., Bryant, R.M., 2005. Ventricular arrhythmia in the X-linked cardiomyopathy Barth syndrome. Pediatr. Cardiol. 26, 632–637.

Steward, C.G., Newbury-Ecob, R.A., Hastings, R., Smithson, S.F., Tsai-Goodman, B., Quarrell, O.W., Kulik, W., Wanders,

R., Pennock, M., Williams, M., Cresswell, J.L., Gonzalez, I.L., Brennan, P., 2010. Barth syndrome: an X-linked cause of fetal cardiomyopathy and stillbirth. Prenat. Diagn. 30, 970–976.

Streckfuss-Bomeke, K., Wolf, F., Azizian, A., Stauske, M., Tiburcy, M., Wagner, S., Hubscher, D., Dressel, R., Chen, S., Jende, J., Wulf, G., Lorenz, V., Schon, M.P., Maier, L.S., Zimmermann, W.H., Hasenfuss, G., Guan, K., 2012. Comparative study of human-induced pluripotent stem cells derived from bone marrow cells, hair keratinocytes, and skin fibroblasts. Eur. Hear. J.

Strogolova, V., Furness, A., Robb-McGrath, M., Garlich, J., Stuart, R.A., 2012. Rcf1 and Rcf2, members of the hypoxia-induced gene 1 protein family, are critical components of the mitochondrial cytochrome bc1-cytochrome c oxidase supercomplex. Mol. Cell. Biol. 32, 1363–1373.

Takeda, A., Sudo, A., Yamada, M., Yamazawa, H., Izumi, G., Nishino, I., Ariga, T., 2011. Eponym: Barth syndrome. Eur. J. Pediatr. 170, 1365–1367.

Tsukihara, T., Aoyama, H., Yamashita, E., Tomizaki, T., Yamaguchi, H., Shinzawa-Itoh, K., Nakashima, R., Yaono, R., Yoshikawa, S., 1996. The whole structure of the 13-subunit oxidized cytochrome c oxidase at 2.8 A. Science 272, 1136–1144.

Valianpour, F., Wanders, R.J.A., Barth, P.G., Overmars, H., van Gennip, A.H., 2002. Quantitative and compositional study of cardiolipin in platelets by electrospray ionization mass spectrometry: application for the identification of Barth syndrome patients. Clin. Chem. 48, 1390–1397.

Valianpour, F., Wanders, R.J., Overmars, H., Vaz, F.M., Barth, P.G., van Gennip, A.H., 2003. Linoleic acid supplementation of Barth syndrome fibroblasts restores cardiolipin levels: implications for treatment. J. Lipid Res. 44, 560–566.

Vukotic, M., Oeljeklaus, S., Wiese, S., Vögtle, F.N., Meisinger, C., Meyer, H.E., Zieseniss, A., Katschinski, D.M., Jans, D.C., Jakobs, S., Warscheid, B., Rehling, P., Deckers, M., 2012. Rcf1 mediates cytochrome oxidase assembly and respirasome formation, revealing heterogeneity of the enzyme complex. Cell Metab. 15, 336–347.

Wenz, T., Hielscher, R., Hellwig, P., Schägger, H., Richers, S., Hunte, C., 2009. Role of phospholipids in respiratory cytochrome bc(1) complex catalysis and supercomplex formation. Biochim. Biophys. Acta 1787, 609–616.

Whited, K., Baile, M.G., Currier, P., Claypool, S.M., 2012. Seven functional classes of Barth syndrome mutation. Hum. Mol. Genet.

Wu, S.M., Hochedlinger, K., 2011. Harnessing the potential of induced pluripotent stem cells for regenerative medicine. Nat. Cell Biol. 13, 497–505.

Xu, Y., Sutachan, J.J., Plesken, H., Kelley, R.I., Schlame, M., 2005. Characterization of lymphoblast mitochondria from patients with Barth syndrome. Lab. Invest. 85, 823–830.

Xu, Y., Malhotra, A., Ren, M., Schlame, M., 2006. The enzymatic function of tafazzin. J. Biol. Chem. 281, 39217–39224.

Ytrehus, K., Myklebust, R., Olsen, R., Mjøs, O.D., 1987. Ultrastructural changes induced in the isolated rat heart by enzymatically generated oxygen radicals. J. Mol. Cell. Cardiol. 19, 379–389.

Zhang, M., Mileykovskaya, E., Dowhan, W., 2002. Gluing the respiratory chain together. J. Biol. Chem. 277, 43553–43556.

Zhang, M., Mileykovskaya, E., Dowhan, W., 2005. Cardiolipin is essential for organization of complexes III and IV into a supercomplex in intact yeast mitochondria. J. Biol. Chem.